Synthesis and Nucleosome Structure of DNA Containing a UV Photoproduct at a Specific Site†

Joseph V. Kosmoski and Michael J. Smerdon*

Department of Biochemistry and Biophysics, Washington State University, Pullman, Washington 99164-4660

Received February 8, 1999; Revised Manuscript Received May 17, 1999

ABSTRACT: A strategy was developed to assemble nucleosomes specifically damaged at only one site and one structural orientation. The most prevalent UV photoproduct, a *cis-syn* cyclobutane thymine dimer (*cs* CTD), was chemically synthesized and incorporated into a 30 base oligonucleotide harboring the glucocorticoid hormone response element. This oligonucleotide was assembled into a 165 base pair double stranded DNA molecule with nucleosome positioning elements on each side of the *cs* CTD-containing insert. Proton NMR verified that the synthetic photoproduct is the *cis-syn* stereoisomer of the CTD. Moreover, two different pyrimidine dimer-specific endonucleases cut ∼90% of the dsDNA molecules. This cleavage is completely reversed by photoreactivation with *E. coli* UV photolyase, further demonstrating the correct stereochemistry of the photoproduct. Nucleosomes were reconstituted by histone octamer exchange from chicken erythocyte core particles, and contained a unique translational and rotational setting of the insert on the histone surface. Hydroxyl radical footprinting demonstrates that the minor groove at the *cs* CTD is positioned away from the histone surface about 5 bases from the nucleosome dyad. Competitive gel-shift analysis indicates there is a small increase in histone binding energy required for the damaged fragment ($\Delta\Delta G \sim 0.15$ kcal/mol), which does not prevent complete nucleosome loading under our conditions. Finally, folding of the synthetic DNA into nucleosomes dramatically inhibits cleavage at the *cs* CTD by T4 endonuclease V and photoreversal by UV photolyase. Thus, specifically damaged nucleosomes can be experimentally designed for in vitro DNA repair studies.

Ultraviolet (UV)[1] radiation damages DNA, generating a variety of different photoproducts (*1*, *2*). Without repair, these lesions give rise to mutations and increase the potential for cancer (*3*). Hence, environmental pressure to maintain the integrity of the genome has given rise to several biochemical mechanisms designed to repair DNA photoproducts and other DNA lesions (*3*−*5*). Indeed, genetic analyses of DNA repair deficient mutants have targeted over 30 genes and gene products required for efficient repair of DNA damage (*6*). However, the variations in photoproduct type, along with differences in DNA location, rates of formation, and associated chromatin structure, complicate biochemical and cellular studies on the repair of these lesions.

A specifically damaged chromatin substrate would be beneficial for a thorough understanding of molecular events associated with DNA repair. Current models for DNA repair in eukaryotes implicate both gene transcription and chromatin structure as modulators of DNA repair in vivo (*7*, *8*). Many actively transcribed regions of class II genes are repaired more efficiently than nontranscribed regions. Closer inspection revealed that the transcribed strands of these genes are repaired more efficiently than the complementary strands, giving rise to the notion of transcription coupled repair (*8*, *9*). Yet, a vast majority of DNA in mature cells is transcriptionally inactive and condensed into heterochromatin (*10*). The challenge to overcome chromatin structure by repair enzymes is exemplified by the fact that naked DNA is more rapidly repaired in cell extracts than the same sequence folded into nucleosomes (*11*, *12*). Moreover, covalent modifications of nucleosome structure, such as histone acetylation, may be required to overcome this packaging and allow entry of repair enzymes into compact regions of chromatin (*13*, *14*). Clearly, there exists a need to develop a well-characterized chromatin substrate for in vitro studies of DNA repair.

An ideal substrate for in vitro DNA repair experiments should allow specific incorporation of DNA lesions at any site in a given DNA sequence. Furthermore, the length of dsDNA should exceed ∼130 bp if a nucleosome template is desired (*15*, *16*). A DNA primary sequence which confers a well-defined translational and rotational setting of the nucleosome is necessary to control structural orientation of the

† This study was supported by NIH Grant ES04106 from the National Institute of Environmental Health Sciences.

* Corresponding author [509-335-6853 (phone)/509-335-9688 (FAX)/smerdon@mail.wsu.edu (e-mail)].

[1] Abbreviations: UV, ultraviolet; *cs* CTD, *cis-syn* cyclobutane thymine dimer; dsDNA, double-stranded DNA; bp, base pairs; SELEX, systematic evolution of ligands by exponential enrichment; GRE, glucocorticoid response element; N, any nucleotide; TLC, normal phase thin-layer chromatography; NMR, nuclear magnetic resonance; IR, infrared; DMT, dimethoxytrityl; TBDMS, *tert*-butyldimethylsilyl; mole eq, mole equivalent; NOE, nuclear Overhauser effect; RPHPLC, reverse phase high-pressure liquid chromatography; EDTA, disodium ethylenediaminetetraacetate; TBE, 90 mM Tris base, pH 8.3, 90 mM borate, 2.5 mM EDTA; BSA, bovine serum albumin; TE, 10 mM Tris, pH 8.0, 1 mM EDTA; PCI, 50% Tris-buffered phenol, 48% chloroform, and 2% isoamyl alcohol; T4 endo V, T4 endonuclease V; cv-PDG, chorella virus pyrimidine dimer glycosylase; PAGE, polyacrylamide gel electrophoresis; PMSF, phenylmethylsulfonyl fluoride; •OH, hydroxyl radical; MW, molecular weight.

10.1021/bi990297h CCC: $18.00
Published on Web 07/02/1999

lesion. Such control of the substrate would greatly facilitate attempts to understand the role of nucleosome structure upon DNA repair. Finally, incorporation of a transcription factor binding site within the DNA sequence may address the consequences of specific DNA lesions on related DNA processing events. In the present paper, we have incorporated each of these sequence characteristics into a novel nucleosome substrate for in vitro DNA repair assays.

Previously, Taylor and co-workers synthesized a *cs* CTD phosphoramidite and incorporated the photoproduct into oligonucleotides (*17, 18*). Using this approach, these investigators addressed several important structural questions concerning UV-damaged DNA and its repair (*19, 20*). Following their lead, we specifically incorporated *cs* CTDs at sites of interest within synthetic oligonucleotides. A major disadvantage of the synthetic approach, however, continues to be the size limitations of synthetic oligonucleotides and requires assembly of smaller fragments in order to generate dsDNAs larger than ~100 bp in length. Despite these limitations, we assembled specifically damaged dsDNA, 165 base pairs (bp) in length, using standard protocols.

Nucleosome positioning elements within the primary sequence have been shown to direct translational and rotational setting of the DNA molecule relative to the core histone octamer (*10, 16, 21*). Moreover, poly A stretches of >5 bases are more rigid than most DNA sequences and may prevent translational sliding of histone octamers (*22*). Recently, SELEX experiments have identified sequences from random DNA libraries with high relative affinity toward nucleosome formation (*23*). One family that emerged from the random population represented an already characterized sequence with a nucleosome positioning element known as the TG motif (*21, 24*). This motif consists of a 10 base repeat of the sequence $(G/C)_3NN(A/T)_3NN$. The alternating A/T and G/C steps cause compression of the minor and major grooves, respectively, at regular (~10 bp) intervals, thus facilitating the bending of DNA around the histone octamer.

We have used the TG motif to rotationally and translationally orient our *cs* CTD within a nucleosome. This study was stimulated by the work of Li and Wrange (*25, 26*), who positioned the glucocorticoid hormone response element (GRE) within the dyad region of a reconstituted nucleosome by bracketing the GRE-containing fragment between tracts of TG motifs. In addition, we integrated poly A stretches of 6 and 7 nucleotides at the ends of the dsDNA fragment to help prevent translational sliding of histone octamers (*22*). We report here that these nucleosome positioning elements can enforce a predetermined nucleosome structure on the central DNA sequence even when it contains an UV photoproduct. Furthermore, we show that nucleosome folding dramatically inhibits enzymatic cleavage and photoreversal at the *cs* CTD.

MATERIALS AND METHODS

Synthesis of cs CTD Phosphoramidite. Commercial reagents were purchased from Aldrich Chemicals and used with no further purification. Normal phase silica gel (230−400 mesh) was obtained from Whatman. Normal phase glass-backed silica gel TLC plates were from EM Separations Technologies. Reaction solvents were appropriately distilled and blanketed with dry argon just prior to use. Synthetic

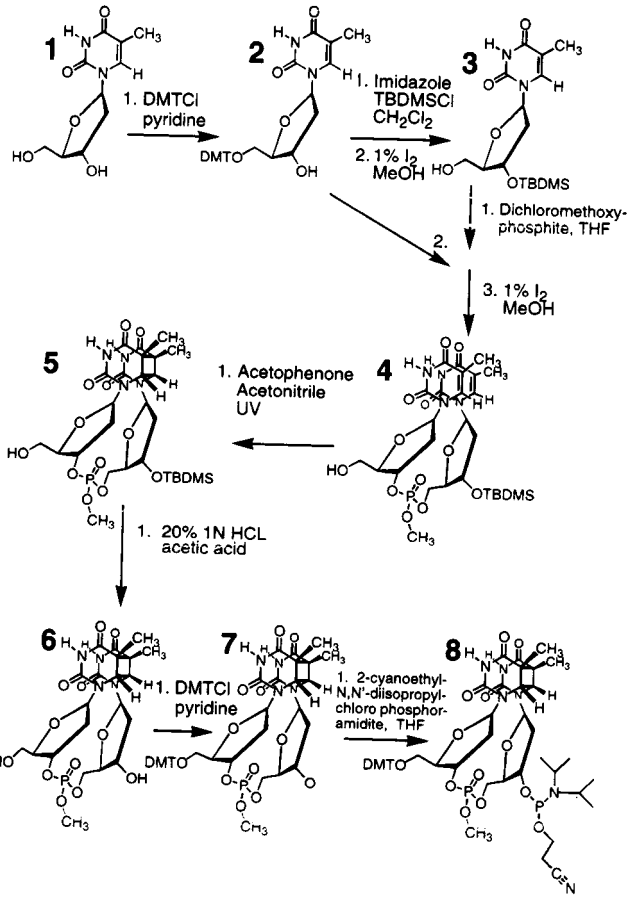

FIGURE 1: Reaction pathway used to synthesize the *cs* CTD phosphoramidite. Numbers in boldface type denote individual products in the synthesis. Abbreviations: DMT, dimethoxytrityl; TBDMS, *tert*-butyldimethylsilyl.

reactions were conducted under anhydrous conditions and inert atmosphere. Reaction yields are reported as an average of three or more experiments. Melting temperatures were measured on a Mel-Temp II apparatus. Routine 1D ^{1}H NMR spectra were collected on a Bruker 300 MHz instrument and referenced to the solvent peak. IR spectra were obtained with a Perkin-Elmer 1600 series spectrometer, and UV spectra were recorded on a Spectronics Genesys II single-beam spectrometer.

The seven step pathway used to obtain the desired *cs* CTD phosphoramidite is presented in Figure 1. Thymine was converted to the respective 5′-dimethoxytrityl derivative (5′DMTdT) utilizing standard protocols (*27*) and purified by crystallization from benzene (Figure 1, product **2**). The known compound, 3′-*tert*-butyldimethylsilyl thymine (3′TBDMSdT), was obtained in a novel one-pot reaction by combining two established protocols (*28, 29*). Briefly, 1.0 mole equivalent (mole eq) of product **2** was combined with 1.1 mole eq of imdazole and then 1.1 mole eq of TBDMSCl in CH_2Cl_2 at a final concentration of 0.5 M (limiting reagent). The reaction flask was fitted with a condenser and heated to 55 °C for 16 h, and then quenched with 0.5 mole eq of MeOH. The crude organic product was washed by means of aqueous extraction, dried by sodium sulfate, and rotary-evaporated to a white foam. Next, 1% iodine in MeOH (*29*) was employed to specifically deprotect the 5′DMT intermediate, rendering product **3**. Normal phase silica gel chromatography was used in conjunction with a step gradient profile

from 1% to 10% MeOH in CH_2Cl_2 to purify 3′TBDMS thymine. Product **3** was converted to the methyl chlorophosphite en route and condensed with product **2** (*30*, *31*) to give the fully protected thymine dimer intermediate. Once again, 1% iodine in MeOH (*29*) was adopted to specifically remove the 5′DMT group from the condensed crude products to yield product **4**. Absolute separation of the free DMT from the product is imperative and was accomplished by gravity flow normal phase silica gel chromatography. The column was packed and loaded with 98% CH_2Cl_2, 1% MeOH, and 1% pyridine, and then eluted until all free DMT was removed. The desired product, **4**, was eluted with 7% MeOH, 93% CH_2Cl_2. Appropriate fractions were combined and concentrated under rotary evaporation using weak vacuum.

Products **5a** through **7** were synthesized as previously described by Taylor and colleagues (*17*, *18*). The final product, **8**, was obtained by combining 1.0 mole eq of product **7** with 4.0 mole eq of *N*,*N*-diisopropylethylamine and 1.2 mole eq of [(2-cyanoethyl)(*N*,*N*-diisopropyl)]chlorophosphoramidite in tetrahydrofuran (1 M) at room temperature and was allowed to react for 42 min (*32*, *33*). A pad of silica was used to isolate product **8** (packed and loaded with 90% ethyl acetate, 9% hexane, and 1% triethylamine, then eluted with ethyl acetate). The *cis-syn* CTD phosphoramidite reagent was dried under high vacuum to yield a clear glass, and then dissolved in dry acetonitrile under argon to give a 0.1 M solution just prior to automated oligonucleotide synthesis (see below).

Observed spectroscopic values for product **8** are as follows: ^{1}H NMR, 7.2−6.8 ppm (m, aromatic DMT), 6.0 ppm (mm), 5.0 ppm (mm), 4.38 ppm (m), 4.1 ppm (d, J = 5.5 Hz, H6), 4.04 ppm (d, J = 6.59 Hz, H6), 3.8 ppm (s, DMT OCH_3), 3.65 ppm (d, J = 12.1 Hz, $POCH_3$), 3.2−2.8 ppm (mm), 1.39 ppm (s, $C5CH_3$), 1.25 ppm (d, J = 4.6 Hz, $isoCH_3$), 1.19 ppm (s, $C5CH_3$); ^{32}P NMR ($CDCl_3$, ppm from TMP), 147.5 ppm 146.8 ppm (2s phosphoramidite), −4.17 ppm, −4.29 ppm (2s phosphate); IR ($CHCl_3$) 2916 cm^{-1}, 2849 cm^{-1}, 2360 cm^{-1}, 1717 cm^{-1}, 1558 cm^{-1}, 1508 cm^{-1}, 1463 cm^{-1}, 1253 cm^{-1}, 1179 cm^{-1}, 1031 cm^{-1}, 706 cm^{-1}; UV ($CHCl_3$), λ_{max} 230 nm, 242 nm, 274 nm, λ_{min} 235 nm, 262 nm, 278 nm; TLC (MeOH 10%/CH_2Cl_2 90%) R_f 0.5.

Structural NMR Experiments. Data were collected on a Varian 500 MHz instrument by Dr. Greg Helms at the Washington State University NMR center. 1D difference ^{1}H NOE experiments (*34*) of product **6** in D_2O at 20 °C were conducted by selective irradiation of the C5 methyl protons at either 1.53 or 1.43 ppm, as well as the C6 cyclobutyl protons (4.25 and 4.01 ppm). The results demonstrated that the vast majority of product **6** has the desired *cis-syn* conformation (data not shown).

Oligonucleotide Synthesis. Oligonucleotides were synthesized by Dr. Gerhard Munske on an ABI 380B automated oligonucleotide synthesizer at the Washington State University Laboratory for Biotechnology and Bioanalysis. Standard protocols for 0.02 μmol scale synthesis were followed with the exception of an extended coupling time of 10 min for the incorporation of the *cs* CTD. Primary sequences for the four oligonucleotides A, B, C, and D are as follows: A is 5′-CGA AAA AAA GTG GAC GAG CGA AGA TGA GAC GGT GTT AGA GCC TGT AAT TCG GTG TTA GAG CCT GTA AT-3′, B is 5′-CCG AAT TAC AGG CTC TAA CAC CGA ATT ACA GGC TCT AAC ACC GTC TCA

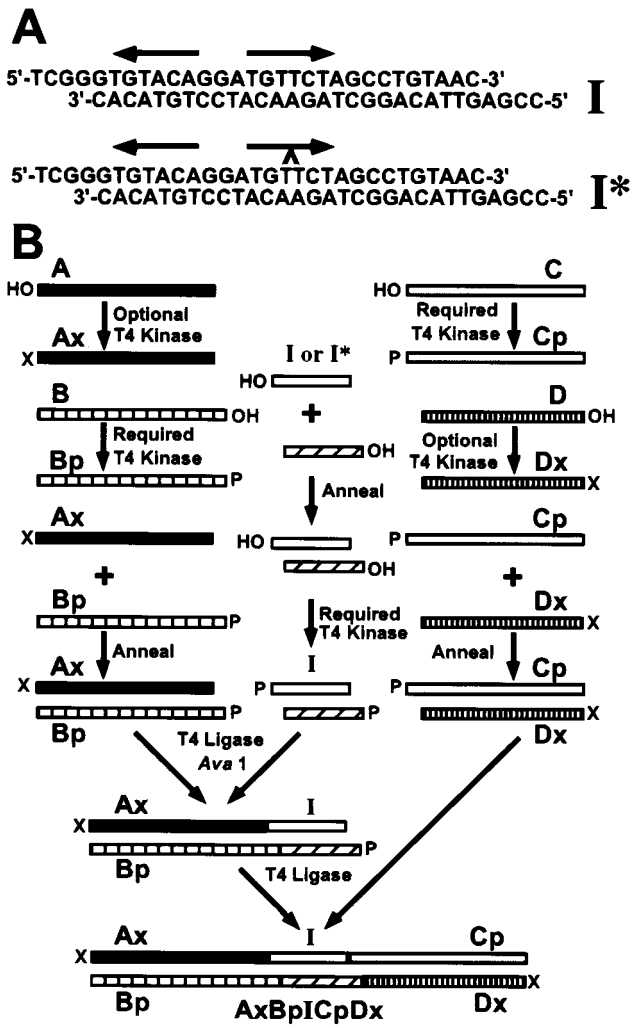

FIGURE 2: Oligonucleotide assembly. (A) Sequences of undamaged (I) and damaged (I*) inserts. The *cs* CTD is designated by a circumflex (ˆ) over the site of incorporation. The bipartite glucocorticoid hormone receptor binding sequence (GRE) is designated by the horizontal arrows. (B) Flowchart depicting assembly of synthetic oligonucleotides into a 165 bp dsDNA. Single-stranded oligonucleotides are appropriately phosphorylated, complimentary sequences are annealed, and the dsDNA oligonucleotides are ligated in a sequential fashion. Sequences AxBp and CpDx contain the nucleosome positioning elements (TG motifs and poly As).

TCT TCG CTG GTC CAC TTT TTT TCG-3′, C is 5′-TCG GTG TAA GAG CCT GTA ATT CGG TGT TAG AGC CTG TAA TAG CCG TTG GCG GAA GGC AAA AAA CGA T-3′, and D is 5′-ATC GTT TTT TGC CTT CCG CCA ACG GCT ATT ACA GGC ACT AAC ACC GAA TTA CAG GCT CTT ACA-3′. The double-stranded undamaged and damaged insert sequences are shown in Figure 2A. Synthetic oligonucleotides were obtained as the base-protected, support-bound, and 5′-tritylated products.

Deprotection of Oligonucleotides. The *cs* CTD containing oligonucleotides were first treated with 20% thiophenol, 40% triethylamine, and 40% tetrahydrofuran as described (*17*, *35*) to remove the methyl protecting group from the phosphate. Next, all oligonucleotides were cleaved from the support in a sealed glass vial for 6 h with concentrated NH_4OH at 55 °C in the dark. The cleavage mixture was concentrated with a stream of argon prior to speed vac evaporation. Crude products were brought up in 1.0 mL water and purified by reverse phase HPLC (RPHPLC).

Purification of Oligonucleotides. Crude tritylated oligonucleotides were purified on a Waters HPLC with a Vydac 214TP1010 semipreparative C4 reverse phase column, using a linear gradient from 5% to 40% acetonitrile in 50 mM triethylammonium acetate. Eluate was monitored at 280 nm, and the appropriate fractions were frozen in liquid nitrogen and lyophilized. The 5′DMT group was removed with 80% acetic acid for 30 min at room temperature. The cleavage mixture was dried in a speed vac evaporator and subjected to a second round of RPHPLC, as described above. Lyophilized oligonucleotide products were dissolved in 1.0 mL of TE buffer (10 mM Tris, 1 mM EDTA, pH 8.0) and stored at −20 °C. Aliquots of single-stranded oligonucleotides were quantified by UV spectroscopy assuming 1.0 $A_{260} = 33$ μg/mL ssDNA.

Electrophoresis of Oligonucleotides. Routine polyacrylamide gel electrophoresis was carried out on a Bio-Rad Mini-Protean II apparatus. Purification of ligation products was carried out on a Bio-Rad Protean II xi electrophoresis apparatus. Sequencing gels were run on a Gibco-BRL Model SA apparatus. All gels were run in TBE buffer (90 mM Tris base, 90 mM borate, 2.5 mM EDTA, pH 8.3). Molecular weight markers used in this study were generated from a *Hpa*II digest of the plasmid SK (Gibco-BRL), to give fragment sizes (in bp) of 713, 489, 404, 367, 242, 190, 147, 118, 110, 67, 57, 34, and 26.

Assembly of Full-Length dsDNA. Figure 2B outlines the strategy used to assemble full-length, 165 bp, dsDNA. The single-stranded synthetic oligonucleotides were phosphorylated at their 5′-hydroxyl with T4 polynucleotide kinase (Gibco-BRL) at 37 °C for 30 min according to the manufacturer's specifications. Phosphorylated oligonucleotides were PCI-extracted, using phase lock gel extractors (purchased from 5Prime→3Prime), and purified on a G50 column (Pharmacia Biotech) in TE buffer. Equal moles of complimentary oligonucleotide sequences (calculated from A_{260}) were annealed at 1.0 M in TE buffer by slow cooling from 95 to 4 °C. Annealing efficiency was monitored by native polyacrylamide gel electrophoresis (PAGE).

Ligation of AxBp to the appropriate insert was accomplished by combining 10 μg of AxBp, 20 μg of the appropriate insert, 20 μL of concentrated reaction buffer, and 5 units of T4 DNA ligase (Gibco-BRL) and incubating at 25 °C for 1 h. The resultant mixture of products was reduced to the desired AxBpI and excess inserts by *Avu*I (Gibco BRL) digest according to manufacturer's specifications. After PCI extraction and ethanol precipitation, AxBpI was isolated from excess insert by native PAGE (10% acrylamide, 0.25% bisacrylamide gel in TBE). Briefly, the bands of interest were excised, nebulized, soaked in 4 volumes of TE buffer overnight at 42 °C, and isolated by Supelco GenElute spin columns. Next, AxBpI was combined with a 1.2 mole eq of the appropriate CpDx sample, 20 μL of concentrated buffer, and 3 units of T4 DNA ligase in a total of 100 μL, which reacted for 1 h at 25 °C. The 165 bp oligonucleotide was again purified by native PAGE, eluted as described above, and stored at −20 °C in TE buffer until needed. DNA was end-labeled with T4 kinase (Gibco-BRL) and [γ-^{32}P]ATP (3000 mCi/mmol), purchased from NEN Life Science Products. Radiolabeled DNA was PCI-extracted and subjected to G50 chromatography as described above. End labeling specificity was checked with *Aci*I (New England BioLabs, see text).

T4 Endonuclease V and cv-PDG Digestions. A typical 20 μL reaction contained 1 ng of ^{32}P-end-labeled dsDNA and 10 ng of either T4 endonuclease V (T4 endo V) or cv-PDG, which was incubated in 50 mM NaCl, 25 mM sodium phosphate, pH 6.8, 10 mM EDTA, and 100 μg/mL BSA for 1 h at 37 °C (*36, 37*).

Kinetic experiments used to compare enzyme activity on naked DNA and nucleosomes were conducted on 1 ng of radiolabeled substrate with 0.1 ng of T4 endo V. Naked DNA samples were mixed with equal concentrations of core particles as for the nucleosome samples. Aliquots from each reaction were removed at appropriate times and stopped by PCI extraction and ethanol precipitated. Samples were assayed by denaturing PAGE (7 M urea, 10% acrylamide, 0.5% bisacrylamide in TBE). Dried gels were exposed to phosphorimager screens and visualized on a Molecular Dynamics (Model 445-P90) PhosphorImager (Sunnyvale, CA). Images were analyzed with ImageQuaNT software (Molecular Dynamics).

Photoreversal of cs CTDs. Kinetic assays were conducted essentially as described previously (*38*). Typically, 10 ng of DNA in 20 μL was combined with an aliquot from a master mix consisting of 10 pg of purified *E. coli* DNA photolyase in 180 μL of photolyase reaction buffer (20 mM phosphate, pH 7.5, 2 mM EDTA, 0.1 mM dithiothreitol, 100 mM NaCl). Naked DNA samples were combined with an equal concentration of core particles as in the nucleosome samples. Reactions were exposed to photoreactivating light (>350 nm), as previously described (*38*). Aliquots from each reaction (20 μL) were removed following different times of irradiation and subjected to proteinase K digestion (Gibco BRL) according to manufacturer's specifications. Samples were extracted with PCI and ethanol precipitated. Dried samples were subjected to T4 endo V digestion (10 ng of enzyme for each nanogram of DNA) in 20 μL of reaction buffer (50 mM NaCl, 25 mM sodium phosphate, pH 6.8, 10 mM EDTA, and 100 μg/mL BSA) for 1 h at 37 °C. Final products were PCI extracted and ethanol precipitated prior to 7 M urea denaturing acrylamide gel electrophoresis.

Nucleosome Reconstitution. Nucleosome core particles were prepared from packed chicken erythrocytes (Lampire Biological Laboratories) following the methods described by Libertini and Small (*39*). Core histones were characterized on SDS−PAGE gels, and found to have no detectable degradation or impurities. Nucleosome reconstitution was typically carried out with 10 ng of radiolabeled DNA (0.1 pmol) and 2 μg of core particles (20 pmol) in a total volume of 50 μL. Initially, the reaction included 1 M NaCl, 1 mM EDTA, and 10 mM Tris (pH 7.5), which was first allowed to equilibrate for 30 min at 25 °C and then for 30 min at 4 °C. The reaction was dialyzed (Spectra/Por Membrane MWCO 6000−8000) against 0.6 M NaCl, 10 mM Tris (pH 7.5), 1 mM EDTA, and 0.2 mM phenylmethylsulfonyl fluoride (PMSF) for 12 h at 4 °C. Finally, the reaction was dialyzed against 50 mM NaCl, 10 mM Tris-HCl, pH 7.5, 1 mM EDTA, and 0.2 mM PMSF for 4 h at 4 °C. For competitive gel-shift experiments, 100-fold less DNA and chicken erythrocyte core particles was used in the same volume, and the reconstitution protocol was identical. Products were assayed by native PAGE (6% acrylamide,

0.2% bisacrylamide in TBE), dried, exposed to a phosphorimager screen for 24 h, and developed. The ratio of bound to free DNA was quantified by ImageQuaNT software and used to calculate association constants (K_a = bound/free). The change in Gibbs free energy due to incorporation of the *cs* CTD was calculated according to $\Delta\Delta G = -RT \ln[K_a(\text{damaged})/K_a(\text{undamaged})]$.

Hydroxyl Radical Footprinting. Approximately 10 000 cpm of appropriately end-labeled DNA was reacted with hydrogen peroxide as described (*40*). Reactions were quenched with glycerol (final concentration 5%), and histones were removed with proteinase K (Gibco BRL). Samples were evaluated on 7 M urea sequencing gels, which were fixed (7% methanol, 7% acetic acid) and dried. The data were visualized on a phosphorimager and analyzed with ImageQuaNT software as described above.

RESULTS

cs CTD Chemical Synthesis. The route used to produce the *cs* CTD phosphoramidite reagent was developed from known literature reactions and products shown in Figure 1. This reaction scheme varies slightly from that reported by Taylor and colleagues (*17*). The unique combination of 3′-hydroxyl protection with TBDMS (*28*) followed by 5′DMT removal (*29*) in a "one pot" reaction increased yields of product **3** by 20% to give 84% ± 2.9%. Similarly, product **4** yields were improved by 15% ± 4.5% via this same method. Synthetic products **2**−**7** and intermediates were compared to, and agreed with, known literature values for the TLC profile, melting temperature, 1D ^{1}H NMR spectra, UV spectra, mass spectra, and IR spectra. Product **6** was tested for the presence of the *cis-syn* stereoisomer by 1D ^{1}H NOE NMR, and the expected NOEs were obtained (data not shown). Furthermore, TNNOSEY of a dodecamer oligonucleotide detected the presence of the *cs* CTD after oligonucleotide synthesis, deprotection, and purification (data not shown).

Oligonucleotide Synthesis and Purification. The *cs* CTD phosphoramidite incorporated into oligonucleotides with high efficiency. There was no significant difference in the RPHPLC chromatograms generated from either the undamaged or the damaged inserts (data not shown). We found similar results for over a dozen different sequences ranging from 12 to 38 nucleotides. HPLC purified products were further characterized on 7 M urea denaturing gels, and >98% of the oligonucleotides migrated as a single band. The resultant impurities appeared as a minor population of deletion products. The inserts harboring the *cs* CTD were further characterized enzymatically to assess the purity of the damaged site (see below).

Assembly and Labeling of Full-Length dsDNA. The flowchart in Figure 2B outlines the protocols used to construct full-length dsDNA. After 5′-phosphorylation and annealing, ligation of AxBp to a 5-fold molar excess of insert gave a series of complex products due to multiple ligations of inserts (Figure 3A, lanes 4 and 8). These products were reduced to the desired AxBpIx and excess insert by *Ava*I digestion (lanes 5 and 9), and there was no detectable difference in the enzymatic efficiency of ligation between damaged and undamaged inserts. It is clear from these data that a vast majority of AxBp is converted to the desired

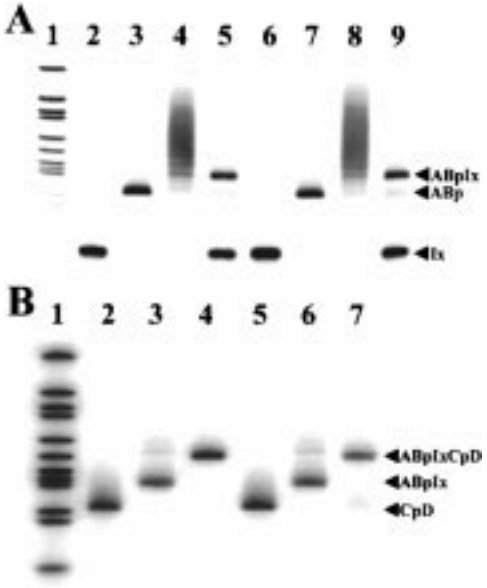

FIGURE 3: Polyacrylamide gel analysis of ligation products. (A) Native gel (10% acrylamide, 0.25% bisacrylamide) showing ligation of inserts to ABp. Samples are: molecular weight markers (lane 1), undamaged insert I (lane 2), ABp (lane 3), ligation products from ABp + I (lane 4), cleavage of ligation products by *Ava*I to ABpI and excess I (lane 5), damaged insert I* (lane 6), ABp (lane 7), ligation products from ABp + I* (lane 8), and cleavage of ligation products with *Ava*I to ABpI* and excess I* (lane 9). Ix represents either insert. (B) Native gel of final ligation products. Samples are: molecular weight markers (lane 1), CpD (lane 2), gel-purified ABpI (lane 3), ABpICpD (lane 4), CpD (lane 5), gel-purified ABpI* (lane 6), and ABpI*CpD (lane 7).

AxBpI product. Efficient ligation of AxBpI to the appropriate CpDx oligonucleotide requires a 5−10% excess of CpDx. Once again, there was no significant difference in products due to the presence of the *cs* CTD (Figure 3B, compare lanes 4 and 7). Since enzyme efficiency was far greater than the purification yields, we recovered 5−10% of the full-length dsDNA from the gel. Thus, starting with 10 μg of AxBp yielded 1−2 μg of full length dsDNA (AxBpICpDx).

Once full-length DNA was assembled, the 5′-hydroxyls were radiolabeled with ^{32}P using the forward reaction of T4 kinase. Prior to assembly, a particular strand was blocked with cold phosphate to prevent radiolabeling of that strand during this step. The specificity of this labeling strategy was checked with *Aci*I, which cuts the full-length DNA into two distinct fragments of 147 and 18 bp. We note that the 18 bp fragment appears as a doublet on native PAGE, due to partial denaturation, and as a single band on 7 M urea denaturing PAGE. Figure 4A shows the *Aci*I digestion products of top (lanes 2 and 3) and bottom (lanes 4 and 5) strand labeled dsDNA after electrophoresis. Although the majority of the desired strand is specifically labeled, there is a small amount (8.1% ± 2.5%) of nonspecific ^{32}P incorporation into the other strand (see lanes 3 and 5).

Comparison of full-length 165 bp products to molecular weight standards (e.g., see Figure 5, lanes 2 and 4) shows reduced mobility of the synthetic DNA on native gels (apparent MW ∼190 bp). This phenomenon is not observed on denaturing gels where the apparent MW is the expected 165 bases (Figure 4A, compare lanes 1 and 2). We attribute the anomalous mobility on native gels to the inherent structure imposed by the TG motifs.

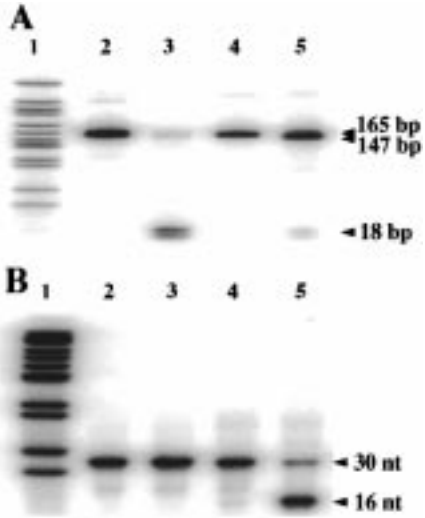

FIGURE 4: Enzymatic characterization of DNA fragments. (A) Native gel showing specificity of ^{32}P end label by *Aci*I digestion. Samples are: molecular weight markers (lane 1), DNA with bottom strand end labeled before (lane 2) and after (lane 3) *Aci*I digest, and DNA with top strand end labeled before (lane 4) and after (lane 5) *Aci*I digest. Arrows denote the full-length (165 bp) DNA and the fragments released by *Aci*I (147 and 18 bp). (B) Denaturing gel of T4 endo V digested undamaged and damaged inserts (I and I*) with the top strand end labeled. Samples are: molecular weight markers (lane 1), undamaged insert before (lane 2) and after (lane 3) T4 endo V digestion, and damaged insert before (lane 4) and after (lane 5) T4 endo V digestion. Arrows denote full-length insert (30 bases) and 16 base fragment released by T4 endo V.

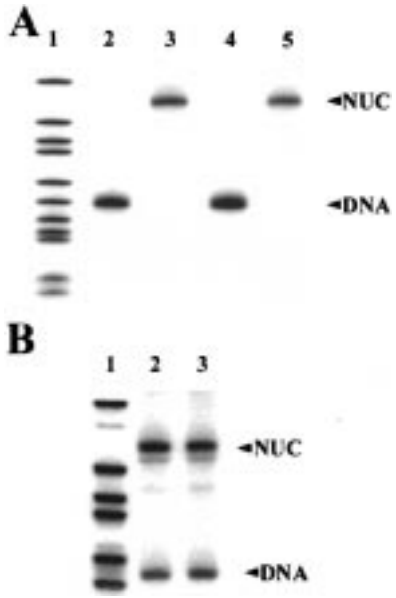

FIGURE 5: Competitive gel-shift analysis of nucleosome reconstitution. (A) Complete nucleosome reconstitution at 200:1 ratio of core particles to full-length DNA fragments. Samples are: molecular weight markers (lane 1), ABpICpD (lane 2), ABpICpD after nucleosome reconstitution (lane 3), ABpI*CpD (lane 4), and ABpI*CpD after nucleosome reconstitution (lane 5). Naked DNA (DNA) and nucleosome (NUC) bands are marked by the arrows. (B) Partial nucleosome reconstitution due to 100-fold dilution of reagents during reconstitution. Samples are: molecular weight markers (lane 1) and reconstitution of undamaged (lane 2) and damaged (lane 3) samples.

Enzymatic Characterization of the 165 bp DNA Fragment Containing a cs CTD. Digestion of DNA with T4 endo V, followed by denaturing gel electrophoresis, was used for identification of UV-damaged DNA. This enzyme makes a single-strand cut specifically at *cis-syn* cyclobutane pyrimidine dimers (*36*, *41*). A representative gel for the T4 endo V digestion of the 30 bp insert with and without the *cs* CTD is shown in Figure 4B. The results indicate that T4 endo V specifically cleaves the inserts at the site of *cs* CTD incorporation (lane 5). Repeat experiments, using several different lots of T4 endo V, indicate the enzyme cuts 92% $\pm$ 3.2% of the inserts from our preparations. Control experiments indicate that the remaining uncut DNA is chemically modified during the many preparation steps.

When these experiments are repeated on full-length dsDNA, even more uncut DNA was observed (see Figure 8A). In this case, 83% $\pm$ 4.1% of the appropriately ^{32}P-end-labeled full-length naked DNA, harboring the *cs* CTD, was cut by T4 endo V. Control experiments indicate that ~8% of the uncut DNA signal is due to nonspecific strand end labeling (see *Aci*I digest; Figure 4A), and the remaining 9% is due to chemical modification of the CTD site during preparation of the oligonucleotides (*17*). In addition, if the damaged DNA is incubated with *E. coli* UV photolyase under photoreversing conditions prior to digestion, to specifically remove *cis-syn* cyclobutane pyrimidine dimers, T4 endo V no longer cuts the DNA (Figure 8B). Control experiments were conducted with the endonuclease cv-PDG in place of T4 endo V. Although cv-PDG has less stereospecificity for substrate (i.e., cuts *trans-syn* II stereoisomers) and enhanced endonuclease activity compared to T4 endo V (*37*), there was no significant increase in the degree of digestion by this enzyme (data not shown). Thus, enzymatic characterization verifies both the position and the stereochemistry of the *cs* CTD in the 165 bp DNA oligonucleotide and indicates ~90% of the expected sites harbor a bona fide *cs* CTD.

Nucleosome Reconstitution. DNA sequences bound histone octamers efficiently during the exchange reaction to give one distinct product on native acrylamide gels (Figure 5A). Our initial conditions were modeled after those used for nucleosome reconstitutions on the 5S ribosomal gene (*42*). These conditions shifted essentially all of the undamaged and damaged DNA to the nucleosome complex (Figure 5A, lanes 3 and 5). Upon a 100-fold dilution of the DNA samples, we observed a small (but significant) preference of the histone octamer for undamaged DNA over the *cs* CTD-damaged DNA. An example of this slight preference is shown in Figure 5B. These experiments were repeated 3 times (with four different core particle to DNA ratios), and association constants were calculated from the ratio of bound to free DNA in each case. An average value of $\Delta\Delta G = +151 \pm 49$ cal/mol was obtained for the difference in free energy between damaged and undamaged DNA. This result indicates there is a small decrease in histone octamer binding energy for the *cs* CTD-damaged DNA, as observed for UV-irradiated *Xenopus borealis* 5S ribosomal DNA (*42*).

Characterization of Nucleosome Structure of the 165 bp Fragment. Hydroxyl radical (·OH) footprinting was used to examine the rotational setting of the DNAs in the reconstituted nucleosomes (*43*). As shown in Figure 6, there is a slight modulation of the ·OH footprint for the naked 165 bp DNA fragment, where the ·OH cutting yields a subtle ~10 base periodicity (Figure 6, lanes 3, 4, 9, and 10). The observed modulation is expected for this sequence as it is

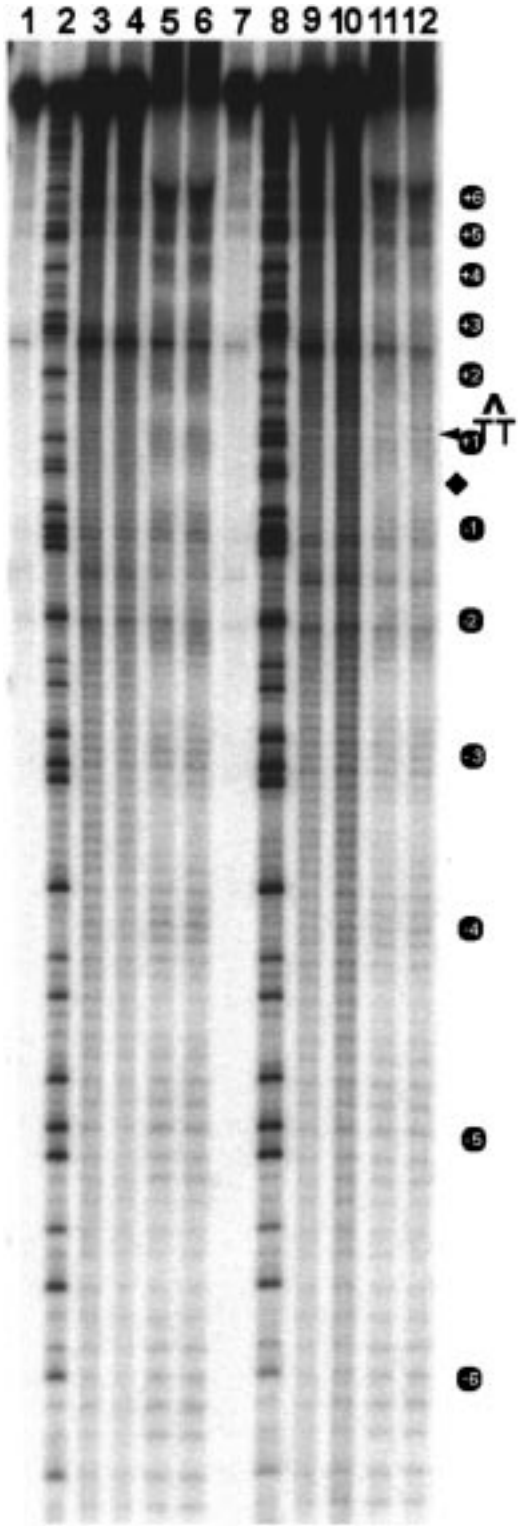

FIGURE 6: Characterization of rotational setting of the full-length fragment in nucleosomes by hydroxyl radical (·OH) footprinting. DNA was ^{32}P-end-labeled on the top strand. Samples are: undamaged fragment ABpICpDp (lane 1), Maxam−Gilbert chemical degradation at Gs in ABpICpDp (lane 2), 2 min (lane 3) and 4 min (lane 4) ·OH digest of naked ABpICpDp, 3 min (lane 5) and 6 min (lane 6) ·OH digest of ABpICpDp nucleosome, damaged ABpI*CpDp (lane 7), Maxam−Gilbert chemical degradation at Gs in ABpI*CpDp (lane 8), 2 min (lane 9) and 4 min (lane 10) ·OH digest of naked ABpI*CpDp, and 3 min (lane 11) and 6 min (lane 12) ·OH digest of ABpI*CpDp nucleosome. Positions of ensemble maxima from ·OH digest are marked and numbered with a ● on the right. The positions of the nucleosome dyad and *cs* CTD are denoted by the ◆ and arrow, respectively.

designed to have periodic bends in the phosphodiester backbone (*24*). When this DNA is folded into a nucleosome, however, the modulation in ·OH cutting is more pronounced [Figure 6, lanes 5, 6, 11, and 12 (ensemble maxima are marked by · and numbered)].

The protection from ·OH cleavage every ∼10 bases indicates there is a distinct rotational setting of DNA in the nucleosome (*15*). Interestingly, there is little difference in the footprints between damaged and undamaged DNAs in nucleosomes (Figure 6, compare lanes 5 and 6 with lanes 11 and 12). Indeed, the only difference observed is at the location of the *cs* CTD (Figure 6, arrow), where a distinct lack of signal occurs in the damaged strand for both naked and complexed DNA (Figure 6, compare lanes 3−6 with lanes 9−12). The "missing band" occurs near the maximum intensity of an ensemble generated by ·OH digest, indicating that the minor groove at the *cs* CTD is oriented away from the histone octamer surface in the reconstituted nucleosome. These results were corroborated by ·OH footprints of nucleosomes radiolabeled on the other DNA strand (data not shown). Two unique bands are also observed in the G sequencing lanes for the damaged DNA, and represent the location of the *cs* CTD (Figure 6, lane 8 and arrow). In agreement with control experiments, we found that the *cs* CTD site is slightly more sensitive to piperidine cleavage at 90 °C than the undamaged DNA fragment, which accounts for these anomalous bands (data not shown). Finally, we note that the unreacted DNAs (Figure 6, lanes 1 and 7) yield some minor bands which migrate at the expected positions of incomplete ligation products, and the ·OH profiles must be corrected for these background signals.

Scans of select lanes from Figure 6 are shown in Figure 7, where the relative signal (i.e., after subtraction of the signal for unreacted naked DNA) is shown. The distinct gap in signal at the *cs* CTD location clearly indicates that the minor groove at the UV photoproduct is rotationally positioned away from the histone surface (Figure 7, scans C and D). These experiments were confirmed with samples labeled on the other strand (data not shown). Finally, the appearance of one predominant nucleosome complex band on 6% native polyacrylamide gels (Figure 5A) suggests a strong preference for a particular translational setting predicted to place the *cs* CTD at position +5 from the nucleosome dyad (*15*, *25*, *26*).

Enzymatic Cleavage and Photoreversal at the cs CTD following Nucleosome Formation. Comparison of enzymatic cleavage by T4 endo V in naked DNA and nucleosomes shows that nucleosome folding of the DNA dramatically decreases endonuclease activity at the *cs* CTD (Figure 8A). For these experiments, great care was taken to ensure equal environments for both samples during the reactions. After quantitation of these gels, comparison of initial slopes of the data indicates that the T4 enzyme activity is reduced by 75−150-fold (Figure 8A, open vs closed circles). Similarly, we observe a marked decrease in photoreversal efficiency by UV photolyase following nucleosome formation (Figure 8). In this case, we observe a 100−400-fold decrease in the yield of *cs* CTD reversal for the same irradiation doses (Figure 8B, open vs closed circles). Thus, nucleosome folding of the full-length DNA dramatically retards these two very different enzyme activities.

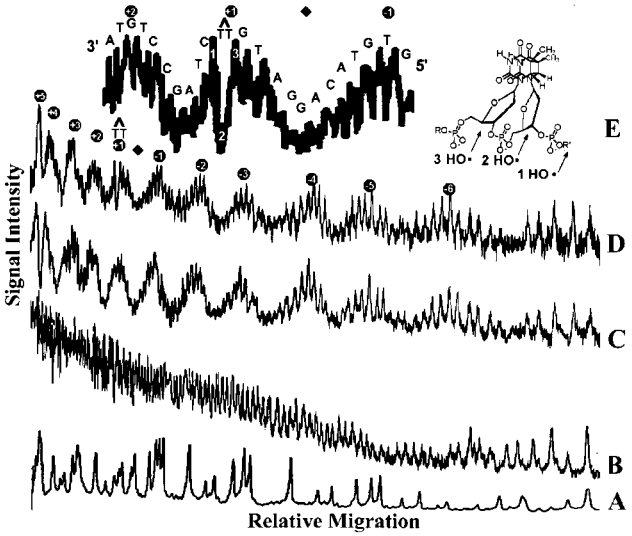

FIGURE 7: Scans of selected lanes of gel in Figure 6. (A) Scan of G sequencing ladder (lane 8) after subtraction of background signal for *cs* CTD-containing DNA (lane 7). (B) Scan of naked damaged DNA ·OH footprint (average of lanes 9 and 10) after subtraction of background signal from *cs* CTD-containing DNA (lane 7). (C) Scan of undamaged nucleosome ·OH footprint (average of lanes 5 and 6) after subtraction of background signal from undamaged DNA (lane 1). (D) Scan of damaged nucleosome ·OH footprint (average of lanes 11 and 12) after subtraction of background signal from *cs* CTD-containing DNA (lane 7). Symbols from gel in Figure 6 (●, ◆, and T T̂) have been transposed over scans D and E to help orient the reader. (E) Enlargement of data from positions +2 to −1 of the damaged nucleosome ·OH footprint containing the *cs* CTD (see Figure 7D). The primary sequence is indicated, and the depression in signal at the *cs* CTD site is denoted by T T̂. Numbers correlate the observed signal to chemical attack by ·OH at the respective ribose moieties.

DISCUSSION

Building on the work of Taylor and co-workers (*17*, *18*), we developed a route to yield a *cs* CTD phosphoramidite reagent (Figure 1). At the heart of this approach is the TBDMS group which allows optimal UV cross-linking and confers chromatographic properties for separation of the resultant stereoisomers. We diverged from Taylor's previous synthesis by utilization of the DMT group for temporary 5′-hydroxyl protection (Figure 1, step 1) prior to UV cross-linking and our choice of phosphoramidite. Taylor and co-workers reported poor cross-linking with DMT derivatives (*17*) and avoided their use until after formation of the desired photoproducts. Initially, we also experienced difficulty cross-linking due to a trace DMT contamination. However, introduction of pyridine into the chromatography solvent allowed for clean separation of the DMT from product **4**, after which cross-linking proceeded as expected. Of a more general interest is our approach to 3′-protected nucleotides (products **3** and **4**). In both cases, the technique of Wahlstrom and Ronald (*29*), using 1% iodine in MeOH, was adapted to specifically remove 5′DMT from the crude products of the previous step in a "one pot" reaction. We attribute our increase in yields of products **3** and **4** to the specificity of this reaction for 5′DMT deprotection, in addition to noticeable reduction in handling. Finally, we preferred to use Letsinger's dichloromethoxyphosphite reagent to condense products **2** and **3** over Ohtsuka's phosphoramidite method due to the facile adaptability of Letsinger's method to large-scale reactions (*31*, *47*).

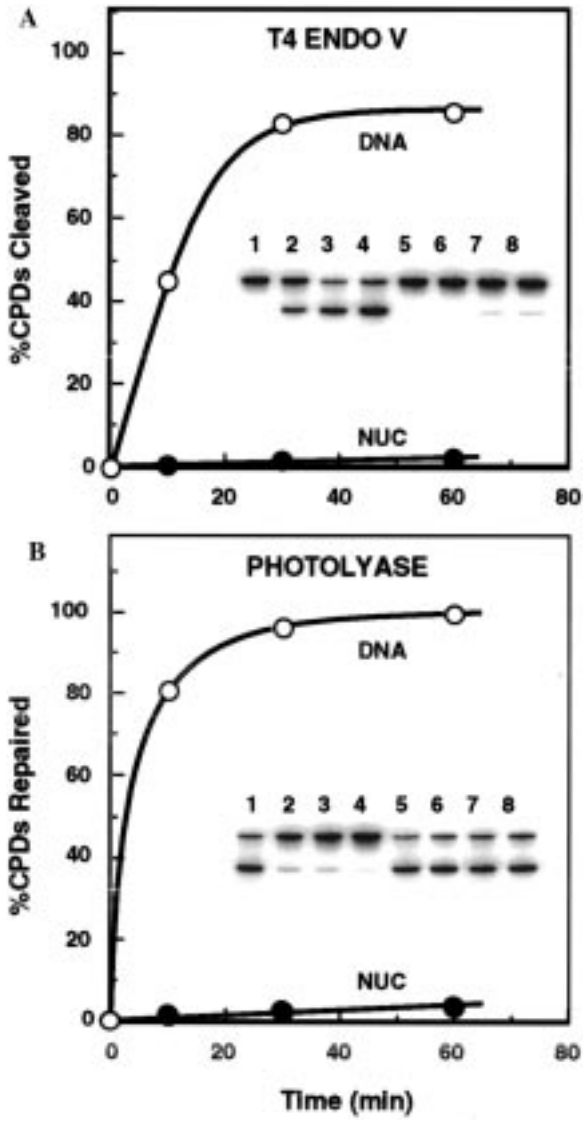

FIGURE 8: Analysis of enzyme reactions on naked DNA and nucleosome substrates. (A) T4 endo V digestion of naked (open circles) and nucleosome (closed circles) substrates. Data represent the average of two experiments. Insert: 7 M urea gel showing T4 endo V cleavage at *cs* CTDs. Samples are naked DNA subjected to T4 endo V for 0, 10, 30, and 60 min (lanes 1−4, respectively), and nucleosome substrate subjected to T4 endo V for 0, 10, 30, and 60 min (lanes 5−8, respectively). (B) Photoreversal of *cs* CTD by *E. coli* UV photolyase on naked (open circles) and nucleosome (closed circles) substrates. Data represent the average of two experiments. Insert: 7 M urea gel showing photoreversal. Samples are naked DNA with photolyase irradiated for 0, 10, 30, and 60 min (lanes 1−4, respectively), and nucleosomes with photolyase irradiated for 0, 10, 30, and 60 min (lanes 5−8, respectively). In each case, samples were subjected to T4 endo V digestion after irradiation to observe remaining *cs* CTDs.

Incorporation of the *cs* CTD into nucleotides showed high yields, not only for the sequences presented in this study but also equally well for a number of other oligonucleotides we have synthesized. Furthermore, no inhibition of reactivity due to steric effects of the *cs* CTD phosphoramidite was observed. We attribute excellent incorporation due to the application of the [(2-cyanoethyl)(*N*,*N*-diisopropyl)]chlorophosphoramidite reagent and meticulous maintenance of anhydrous conditions.

Because the full-length (165 bp) dsDNA could not be amplified through PCR or a biological host (due to the *cs*

CTD), sequential ligation of synthetic oligonucleotides and subsequent strand-specific labeling were used (Figure 4B). Key factors which contributed to the success of this protocol are (a) the unidirectional nature of the insert, (b) specific reduction of multimeric ligation products by *Ava*I to give a single insert product, (c) excellent reactivity of the enzymes on the synthetic DNA substrates, and (d) optimization of reaction temperature at 25 °C to eliminate blunt end ligations.

The synthetic DNA products were subjected to several biochemical assays to verify the presence of the *cs* CTD. Both T4 endo V and cv-PDG enzymes cut 91% ± 2% of the damaged DNA, suggesting a vast majority of the DNA molecules harbor a *cs* CTD. Although cv-PDG has a wider range of enzymatic activity than T4 endo V, it did not cut more of the damaged substrates, suggesting that the uncut species are not other CTD stereoproducts (*37*). Moreover, reversal by the stereospecific *E. coli* photolyase (*44*) was complete, corroborating the results with T4 endo V and cv-PDG. Numerous controls were used to try to identify the structure of the 10% of DNA molecules that were resistant to T4 endo V digestion. However, none of these experiments resolved the structure of these products. Therefore, there may be a minor population of impurities arising from reversal of the *cs* CTD during the many chemical steps in their purification as reported previously by Taylor (*17*).

The primary sequence of insert DNA used in this study contained 15 bp of the glucocorticoid hormone response element (GRE), the *cs* CTD, and nucleosome positioning elements (TG motif) on each side of this CTD-containing insert (Figure 4A). The TG motif confers a distinct rotational positioning of the DNA on the core histones, which gives rise to a unique nucleosome structure (*23*, *25*, *26*). Furthermore, poly A sequences of 6 or 7 bases were incorporated at both ends of the DNA to limit translational migration of the histones (*22*). With the placement of the *cs* CTD at position +5 from the dyad axis of the nucleosome, we predicted the minor groove at the *cs* CTD would be rotationally positioned away from the histone surface (*15*, *26*). This prediction was confirmed for both damaged and undamaged DNA. Both sequences loaded the core histones efficiently, and the reconstitutions routinely yielded just one major product band (Figure 5A), indicating one dominant translational setting (*15*, *42*). In addition, hydroxyl radical footprinting supported the outward rotational setting of the *cs* CTD (Figures 6 and 7). We also observe an absence of signal at the *cs* CTD site (Figure 6) which is explained by the fact that cleavage of the DNA backbone between the two cross-linked thymines would not release a fragment because of the covalent attachment at the cyclobutyl ring (see Figure 7E). This effect has not been observed previously in heterogeneously damaged nucleosome substrates.

The effect of the *cs* CTD on nucleosome reconstitution was addressed by calculation of association constants and $\Delta\Delta G$. Although the experiments yielded substantial variability (i.e., a standard deviation of almost 30%), we detect a small yet significant inhibition by the *cs* CTD on nucleosome formation (about +0.15 kcal/mol). The preference for undamaged DNA over *cs* CTD-containing DNA was observed in each experiment despite this variation. These observations agree with previous experiments on heterogeneously damaged DNA (*42*, *45*, *46*).

Nucleosome folding of the damaged DNA had a dramatic effect on T4 endo V and UV photolyase activity. The data indicate that there is a 100−400-fold decrease in enzyme activity due to nucleosome formation (Figure 8). This is not surprising since these prokaryotic or phage enzymes do not interact with nucleosomes in vivo. Furthermore, these results corroborate previous observations made with heterogeneously damaged DNA (*11*, *12*, *48*). It is worth noting that this sequence of DNA gives rise to an unusually well positioned and stable nucleosome. Therefore, the observed inhibition of these enzymes may represent the upper limit of inhibition by nucleosome formation.

In conclusion, these results demonstrate the feasibility of synthesizing homogeneously damaged nucleosomes. To our knowledge, this is the first report of incorporation of a UV photoproduct at a specific position within a nucleosome. Although the focus of this study is the *cs* CTD, other DNA lesions could be analogously incorporated into nucleosomes using this same positioning strategy. These model nucleosomes should serve as unique substrates for DNA repair experiments to address specific questions concerning the role of chromatin structure in DNA repair.

ACKNOWLEDGMENT

We thank Dr. R. Stephen Lloyd for supplying T4 endonuclease V and cv-PDG, Dr. Aziz Sancar for providing *E. coli* DNA photolyase, Dr. Gerhardt Munske for performing the oligonucleotide synthesis, and Dr. Greg Helms for performing the structural NMR experiments. We also thank Dr. Raymond Reeves, and Dr. Kevin Bertrand, Mark Nissen, Christine Suquet, and members of the Smerdon laboratory for technical help and critical discussions.

REFERENCES

1. Cadet, J., Anselmino, C., Douki, T., and Voituriez, L. (1992) *J. Photochem. Photobiol. B: Biol. 15*, 227−298.
2. Wang, S. Y. (1976) *Photochemistry and Photobiology of Nucleic Acids*, Vol. 1, Academic Press, New York.
3. Friedberg, E. C., Walker, G. C., and Siede, W. (1995) *DNA Repair and Mutagenesis*, ASM Press, Washington, D.C.
4. Sancar, A. (1996) *Annu. Rev. Biochem. 65*, 43−81.
5. Wood, R. D. (1996) *Annu. Rev. Biochem. 65*, 135−167.
6. Sancar, A. (1995) *Annu. Rev. Genet. 29*, 69−105.
7. Smerdon, M. J., and Thoma, F. (1998) in *DNA Damage and Repair* (Nickoloff, J. A., and Hoekstra, M. F., Eds.) Vol. 2, pp 199−220, Humana Press Inc., Totowa, NJ.
8. Mellon, I., Spivak, G., and Hanawalt, P. (1987) *Cell 51*, 241−249.
9. Mellon, I., and Hanawalt, P. (1989) *Nature 342*, 95−98.
10. Wolffe, A. (1995) *Chromatin Structure and Function*, Academic Press, New York.
11. Wang, Z., Wu, X., and Friedberg, E. C. (1991) *J. Biol. Chem. 266*, 22472−22478.
12. Sugasawa, K., Masutani, C., and Hanaoka, F. (1996) *J. Biol. Chem. 268*, 9098−9104.
13. Wade, P., Pruss, D., and Wollfe, A. (1997) *Trends Biochem. Sci. 22*, 128−132.
14. Ramanathan, B., and Smerdon M. J. (1989) *J Biol. Chem. 264*, 11026−11034.
15. Luger, K., Mader, A., Richmond, R., Sargent, D., and Richmond, T. (1997) *Nature 389*, 251−260.
16. van Holde, K. E. (1989) *Chromatin*, Springer-Verlag, New York.
17. Taylor, J., Brockie, I. R., and O'Day, C. L. (1987) *J. Am. Chem. Soc. 109*, 6735−6742.

18. Taylor, J., and Brockie, I. R. (1988) *Nucleic Acids Res. 16*, 5123−5137.
19. Kim, S. T., Malhotra, K., Smith, C. A., Taylor, J., and Sancar, A. (1993) *Biochemistry 32*, 7065−7068.
20. Wang, C., and Taylor, J. (1991) *Proc. Natl. Acad. Sci. U.S.A. 88*, 9072−9076.
21. Shrader, T., and Crothers, D. (1990) *J. Mol. Biol. 216*, 69−84.
22. Nelson, H., Finch, J., Luisi, B., and Klug, A. (1987) *Nature (London) 330*, 221−226.
23. Lowery, P., and Widom, J. (1998) *J. Mol. Biol. 276*, 19−42.
24. Shrader, T. E., and Crothers, D. M. (1989) *Proc. Natl. Acad. Sci. U.S.A. 86*, 7418−7422.
25. Li, Q., and Wrange, O. (1993) *Genes Dev. 7*, 2471−2482.
26. Li, Q., and Wrange, O. (1995) *Mol. Cell. Biol. 15*, 4375−4384.
27. Schaller, H., Weimann, G., Lerch, B., and Khorana, H. A.-(1963) *J. Am. Chem. Soc. 85*, 3821−3827.
28. Ogilvie, K. K. (1973) *Can. J. Chem. 51*, 3799−3809.
29. Wahlstrom, J. L., and Ronald, R. C. (1998) *J. Org. Chem. 63*, 6021−6022.
30. Smith, D., Ogilvie, K., and Gillen, M. (1990) *Tetrahedron Lett. 21*, 861−864.
31. Letsinger, R., and Lunsford, W. (1976) *J. Am. Chem. Soc. 12*, 3655−3661.
32. McBride, L. J., and Caruthers, M. H. (1983) *Tetrahedron Lett. 24*, 245−248.
33. Sinha, N. D., Biernat, J., McManus, J., and Koster, H. (1984) *Nucleic Acids Res. 12*, 4539−4557.
34. Sanders, J., and Hunter, B. (1989) *Modern NMR Spectroscopy*, Oxford University Press, New York.
35. Kieczykowski, G., and Schlesinger, H. (1978) *J. Am. Chem. Soc. 100*, 1938−1941.
36. Dodson, M. L., and Lloyd, R. S. (1989) *Mutat. Res. 218*, 49−65.
37. McCullough, A. K., Romberg, M. T., Nyaga, S., Wei, Y., Wood, T. G., Taylor, J., Van, J., Dodson, M. L., and Lloyd, R. S. (1998) *J. Biol. Chem. 273*, 13136−13142.
38. Gale, J. M., and Smerdon, M. J. (1990) *Photochem. Photobiol. 51*, 411−417.
39. Libertini, L. J., and Small, E. W. (1980) *Nucleic Acids Res. 8*, 3517−3534.
40. Revzin, A. (1993) *Footprinting of Nucleic Acid Complexes*, Academic Press Inc. New York.
41. Lloyd, R., and Linn, S. (1993) in *Nucleases Vol. 2* (Linn, S., Lloyd, R. and Roberts, R. Eds.) pp263−316, Cold Spring Harbor Laboratory Press, Cold Spring Harbor, NY.
42. Mann, D., Springer, D., and Smerdon, M. J. (1997) *Proc. Natl. Acad. Sci USA 94*, 2215−2220.
43. Hayes, J., Tullius, T., and Wollfe, A. (1990) *Proc. Natl. Acad. Sci. U.S.A. 87*, 7405−7409.
44. Husain, I., Sancar, G., Holbrook, S., and Sancar, A. (1987) *J. Biol. Chem. 262*, 13188−13197.
45. Suquet, C., and Smerdon, M. J. (1993) *J. Biol. Chem. 268*, 23755−23757.
46. Matsumoto, H., Takakusu, A., and Ohnishi T. (1994) *Photochem. Photobiol. 60*, 134−138.
47. Murata, T., Iwai, S., and Ohtsuka, E. (1990) *Nucleic Acids Res. 24*, 7279−7286.
48. Schieferstein, U., and Thoma, F. (1998) *EMBO J. 17*, 306−316.

BI990297H